A&A 366, 215–228 (2001)
DOI: 10.1051/0004-6361:20000201

Astronomy & Astrophysics

The "rotation-activity connection": Its extension to photospheric activity diagnostics

S. Messina[1], M. Rodonò[1,2], and E. F. Guinan[3]

[1] Catania Astrophysical Observatory, Via S. Sofia 78, 95125 Catania, Italy
e-mail: sme@sunct.ct.astro.it
[2] Dept. of Physics and Astronomy, University of Catania, Via S. Sofia 78, 95125 Catania, Italy
e-mail: mrodono@alpha4.ct.astro.it
[3] Dept. of Astronomy and Astrophysics, Villanova University, Villanova 19085, PA, USA
e-mail: edward.guinan@villanova.edu

Received 19 May 1999 / Accepted 25 October 2000

Abstract. In this paper we present the results of a different approach in the study of the so-called *rotation-activity connection*, which is a well established correlation between rotation and magnetic activity at chromospheric and outer atmospheric levels. The present study concerns the photospheric level and was carried out by using V-band photometric light curve amplitudes as indicators of starspot coverage and of magnetic activity. A high degree of correlation between the envelope of maximum V-band light curve amplitudes and the rotation period is found for the active star members of young open clusters (IC 2602, IC 2391, Alpha Persei, Pleiades and Hyades), as well as for active field stars. This correlation shows a different behaviour in two different rotation period ranges. Moreover, some evidence of a possible activity "saturation" is found among the most rapidly rotating stars of the sample. Additional correlations between photospheric and other magnetic activity indicators in the chromosphere, transition region and corona are also investigated. The results presented here can be considered as an extension of the well established *rotation-activity connection* valid from the corona, transition region and chromosphere, down to the photosphere.

Key words. stars: activity – late-type – magnetic fields – rotation – starspots

1. Introduction

The cool starspots that appear on the photospheres of stars characterised by high angular momentum and convective envelopes (F–M) are thought to be produced, as on the Sun, by the emergence into the photosphere of bundles of magnetic flux tubes generated in the stellar interior by magnetodynamic processes. The dynamo mechanism is believed to originate near the base of the convective envelope (Parker 1979; Schüssler 1983). Since starspots are the sites of strong magnetic fields, the total percent area covered by spots can provide an indirect measure of the magnetic filling factor (f_S) by spots. The filling factor (f_S) is the fraction of the photosphere covered by magnetic fields confined to spots, and a measure of the total magnetic flux density in spots ($f_S B$), if the magnetic field intensity (B) is known. Other important sites of magnetic fields on the stellar photosphere are bright plages and network elements of total percent area f_P. The covering factor of spots and plages ($f_T = f_S + f_P$) represents a direct measure of the total magnetic filling factor. In contrast to starspots and bright plages, other magnetic activity indicators, such as chromospheric and TR's emission line fluxes, can actually provide only an indirect estimate of the magnetic field (Pallavicini 1992).

Because the value of f_T is related to the total magnetic energy that the dynamo action can provide, it appears to be a suitable parameter for investigating the dependence of the dynamo action on global stellar parameters. Estimates of f_S can be obtained from photometric data by light curve inversion methods based on recently developed "spot models" (Rodonò et al. 1995; Lanza et al. 1998). Non-polarimetric methods, based on the comparison of the broadening excess of Zeeman sensitive with respect to Zeeman insensitive lines (e.g., Mathys 1989; Saar 1990, 1996), are quite successful in determining the properties (total flux density and f_P) of bright magnetic photospheric regions, but are not applicable to dark photospheric regions. Moreover, the spot contribution to the line profile is negligible at optical wavelengths, compared with the contribution of bright magnetic regions.

Send offprint requests to: S. Messina

In this paper we propose to estimate the magnetic filling factor (f_S) from photometric data. We accomplish this by using a parameter which is closely related to the total fractional area covered by starspots: the maximum peak-to-peak amplitude of the optical-band flux rotational modulation. These newly determined values of f_S for a sample of single active late-type stars are used to study the dependence of the fraction of photospheric magnetic activity, confined to dark spots, on global stellar parameters and, in particular, to investigate the *rotation-activity connection* at the photospheric level.

2. Maximum light curve amplitude as an activity indicator

Since photospheric spots are the sites of strong magnetic fields, the convective transport of heat is strongly inhibited and this is the reason why the spots appear darker than the surrounding photosphere. Therefore, cool spots can produce the observed optical flux modulation as they travel across the visible hemisphere and disappear behind the limb of a rotating star.

The amplitude of the modulation depends on several geometrical and physical parameters. Some parameters are constant in time, such as the inclination of the star's rotation axis; or can be assumed to be constant, such as the brightness contrast between spot and photosphere; others are variable, such as the total area covered by spots and their surface distribution. The photometric precision of presently available observations generally does not allow us to distinguish between single huge stellar spots or compact groups of small solar-like spots. Let us briefly summarise the effects of these various parameters on the light modulation amplitude:

- *inclination of the stellar rotation axis and latitude of the spot:* the modulation amplitude depends on both the inclination (i) of the star's rotation axis and the latitude where the spots or spot groups are centred, as can be inferred from the following two extreme cases:
  a) "*pole-on*" star ($i = 0°$): any spot is equally visible at all rotation phases and, therefore, spots can not produce any rotational modulation of the observed flux;
  b) "*equator-on*" star ($i = 90°$): except polar caps, spots are carried by the rotation from a maximum visibility, at the disk centre line, to a minimum visibility, when they disappear from view; while approaching the stellar limb, the limb-darkening effect further depresses the spot's brightness contrast with respect to the photosphere; hence, equatorial spots on *equator-on* stars produce the highest amplitude modulation;

- *temperature and colour indices:* the amplitude of the modulation depends also on the ratio between spot and photospheric brightness or temperature. This ratio is likely to be constant in time and time sequences of light curves of several stars have been successfully modelled (e.g., Rodonò et al. 1995; Lanza et al. 1998; Messina et al. 1999a, 1999b) without any need of changing this ratio. Nevertheless, there exists some indication that this ratio may be variable for different types of stars (Byrne et al. 1995; O'Neal et al. 1998). In the case of the Sun, the spot temperature is inversely correlated to the spot area (Kopp & Rabin 1992). The reddening of the colour indices at light minima, i.e. when the maximum fraction of the projected stellar disk is covered by spots, suggests that, although the spot temperatures are lower than the photospheric temperature, their temperature is several hundreds of degrees K, otherwise the spots would not be able to produce any variation of the colour indices;

- *spot areas and longitudes:* the amplitude of the modulation depends on both the total fractional area covered by spots and on the asymmetry of their longitudinal distribution; the absence of flat maxima in most of the observed light curves and the long-term variation of the brightness maximum suggest that the fraction of the photosphere covered by spots (f_S) can be considered as the sum of two terms: f_u and f_{as},

$$f_S = f_u + f_{as} \leq 1 \quad (1)$$

where f_u represents the minimum areal fraction of spots which are always visible and, therefore, unable to produce any flux modulation, though the star's brightness appears somewhat depressed. In *equator-on* stars ($i = 90°$), we expect bands of spots evenly distributed in longitude and/or polar caps to contribute to f_u. In non *equator-on* stars ($i < 90°$) we may expect an additional contribution from polar spots. At any given epoch, f_u determines the difference (ΔV_u) between the presumed "unspotted" (brightest) magnitude and the "spotted" magnitude at the light curve maximum. Hereafter, the V-band will be considered as an illustrative example.
The parameter f_{as} represents the fraction of spots which are asymmetrically distributed in longitude and are responsible of the flux modulation. Their distribution and total area determine the light curve shape and mean magnitude, respectively. Thus f_{as} determines the peak-to-peak light curve amplitude (ΔV_{as}). Therefore, the total brightness variation (ΔV) from the presumed unspotted level

$$\Delta V = \Delta V_u + \Delta V_{as} \quad (2)$$

may be used to estimate the total spotted area (uniformly + asymmetrically distributed in longitude components) at any given epoch.
However, it must be pointed out that for active stars, such as those analysed in this paper, a completely unspotted level will possibly never become observable. In fact, even the much less active Sun shows a few

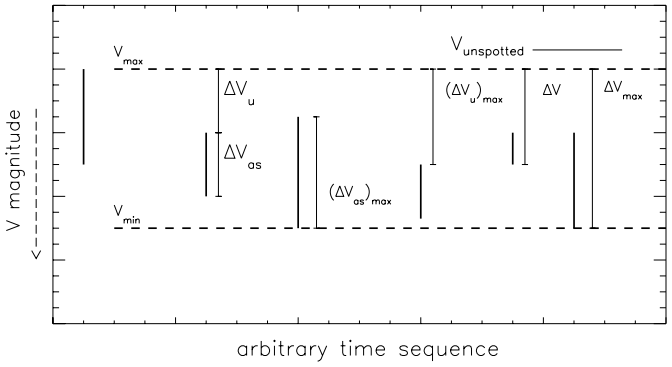

Fig. 1. An illustrative sample of light curve amplitudes (heavy solid bars) is represented to show the meaning of the symbols used in the text: (*from left to right*) $V_{\max}$ and $V_{\min}$ are the star's brightest and faintest magnitudes ever observed; $\Delta V_{\rm as}$ is the observed light curve amplitude and $\Delta V_{\rm u}$ is the difference between the brightest magnitude and the light curve maximum at a given epoch; $(\Delta V_{\rm as})_{\max}$ and $(\Delta V_{\rm u})_{\max}$ are their maximum historic values, respectively; ΔV is the difference between $V_{\max}$ and the light curve minimum at a given epoch; $\Delta V_{\max}$ is the maximum value of the difference between $V_{\max}$ and the faintest magnitude ($V_{\min}$) ever observed; $V_{\rm unspotted}$ is the magnitude corresponding to a completely unspotted visible hemisphere, that may, but does not necessarily, coincide with $V_{\max}$

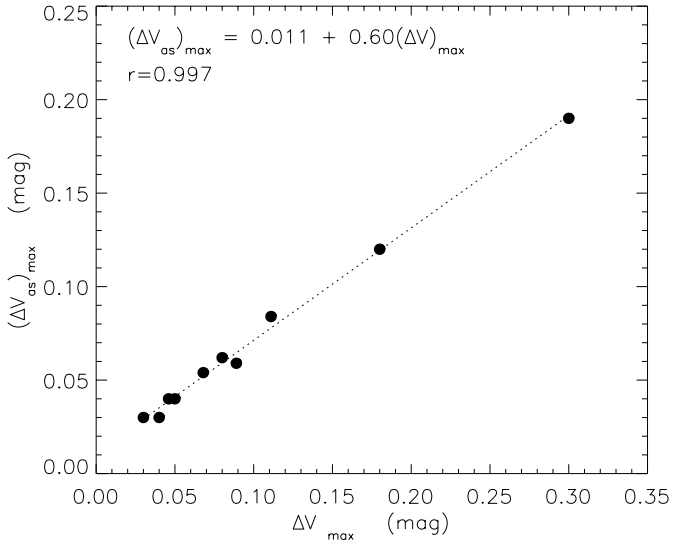

Fig. 2. $(\Delta V_{\rm as})_{\max}$ vs. $\Delta V_{\max}$ for a sample of extensively observed single active stars (Table 8). The dotted line is the fitting linear relation

spots at its activity minimum. Hence, the brightest observed magnitude ($V_{\max}$) may differ (see Fig. 1) from the true unspotted magnitude (Neff et al. 1995; O'Neal et al. 1996) and $\Delta V_{\rm u}$ and ΔV must be considered as lower limits of the uniformly distributed ($f_{\rm u}$) and of the total fraction ($f_{\rm S}$) of spotted area, respectively, at any given epoch. Only from a large number of light curves covering a sufficiently extended time interval the value of $V_{\max}$ can reliably approach $V_{\rm unspotted}$.

Since bright plages may compensate at some level the light dimming effects of dark spots, the value of $\Delta V_{\rm as}$ must be considered as a lower limit of the asymmetrically distributed spotted area. However, for the most active stars at least, the effect of starspots dominates (Radick et al. 1989, 1998) and generally plages are not required to obtain quite satisfactory model light curves (Messina et al. 1999a, 1999b; Lanza et al. 1998; Rodonò et al. 1995), so that plage contamination was disregarded in the present study.

On the basis of these considerations $\Delta V = \Delta V_{\rm u} + V_{\rm as}$ represents a lower limit on the total spot covering fraction ($f_{\rm S}$), that approaches the true value if an extended long term study is available.

We believe that the amplitude of the long-term variation ($\Delta V_{\max} = V_{\max} - V_{\min}$), the maximum values of $\Delta V_{\rm u}$ and $\Delta V_{\rm as}$ [$(\Delta V_{\rm u})_{\max}$ and $(\Delta V_{\rm as})_{\max}$, respectively] obtained from an extended time series of light curves represent the best estimates (though certainly lower limits) of the maximum spottedness ($f_{\max}$) and of the extreme values of the uniform ($f_{\rm u}$) and asymmetric ($f_{\rm as}$) components of the spotted area on a given star. A graphic illustration of the parameters we use in this section is presented in Fig. 1.

By analysing a sample of single late-type stars with rather extended time series of light curves (see Table 8), it has been noted (Messina 1998) that $(\Delta V_{\rm as})_{\max}$ increases with increasing total spotted area ($\Delta V_{\max}$). The existence, at least for extensively observed single stars, of such a strong correlation between $(\Delta V_{\rm as})_{\max}$ and $\Delta V_{\max}$, as shown in Fig. 2, indicates that not only $\Delta V_{\max}$, but also the light curve maximum amplitude $(\Delta V_{\rm as})_{\max}$ from time series of light curves can be adopted as suitable indicator of a lower limit of the star maximum spottedness ($f_{\max}$).

The last result is very important if we consider that the value of $\Delta V_{\max}$, which most closely approaches $V_{\rm unspotted}$, has been measured for a small sample of stars, whereas the value of $(\Delta V_{\rm as})_{\max}$, which does not depend on $V_{\rm unspotted}$, is obviously available for a much larger sample of stars.

3. Analysis and discussion

For the present study we selected from the literature a sample of 225 active single stars according to the following criteria: a) single main-sequence stars, because it is not clear, yet, how both binarity and evolution of the internal structure outside of the main sequence influence the magnetic activity; b) stars belonging to stellar clusters of known age (IC 2391, IC 2602, Alpha Persei, Pleiades and Hyades clusters) in order to study age effects on the magnetic activity, as well field stars; c) stars with known rotation periods; d) stars with well determined light curve amplitudes (in the V-band of the Johnson's UBV system) (Tables 3–8).

In an earlier study by O'Dell et al. (1995) the dependence of the light curve amplitude on the rotation period and on the inverse Rossby number (R ($\equiv {R_0}^{-1}$) $= \tau_{\rm c}/P$, where $\tau_{\rm c}$ is the convective turnover time at the base of the

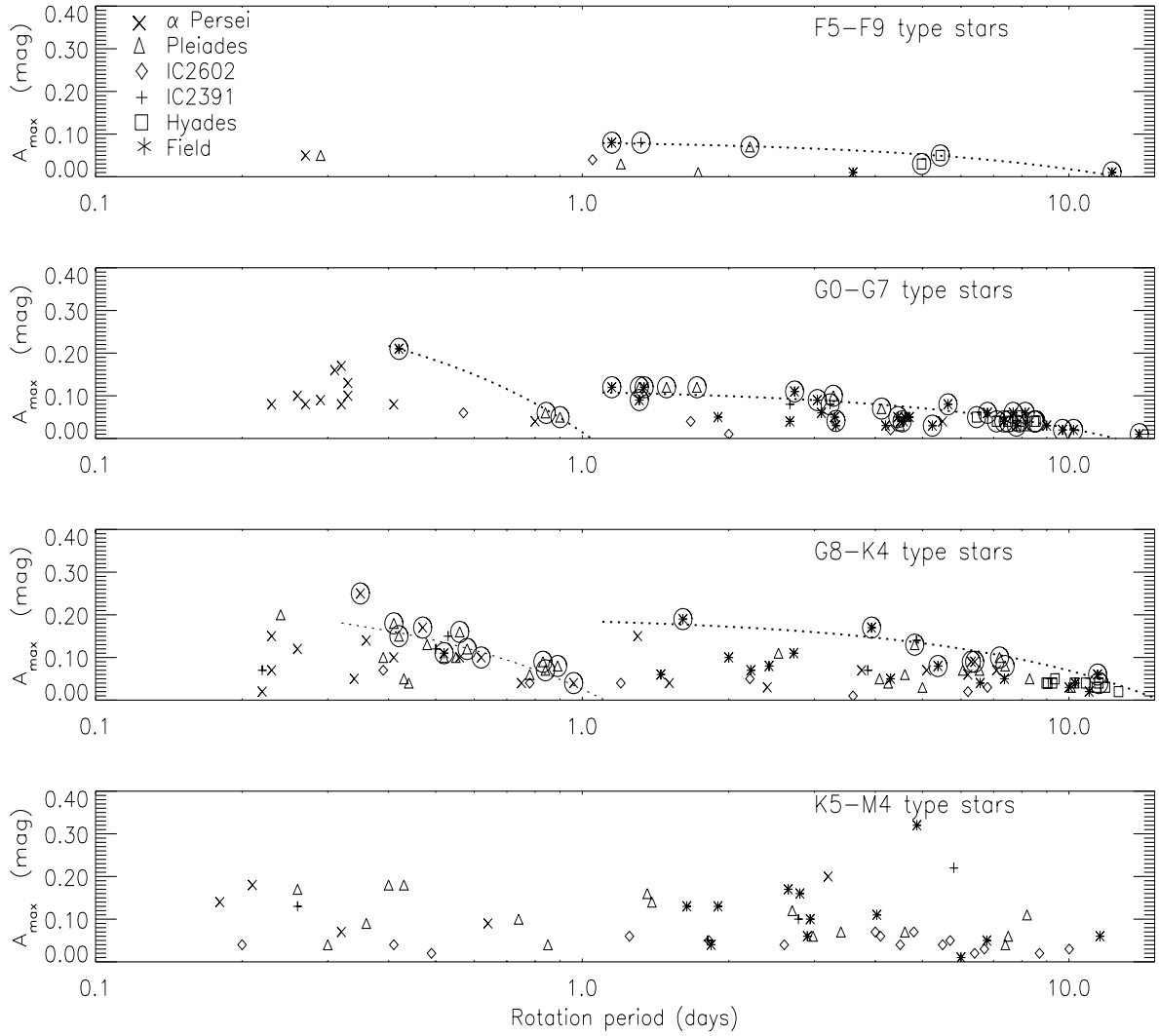

Fig. 3. $A_{\max}$ versus rotation period (P). The data upper envelopes (circled symbols) both in the *ultra fast* and *fast* rotation ranges are best fitted (*dotted line*) by a linear law for F, G and K-type stars. Note that the abscissa is logarithmic

Table 1. The Rossby number (R_0) ranges in which different slopes can be identified, as shown in Fig. 4

type	*ultra fast*	*fast*
F		$R_0 > 0.18$
G	$R_0 \leq 0.10$	$R_0 > 0.10$
K	$R_0 \leq 0.06$	$R_0 > 0.06$

convection zone) was suggested on qualitative grounds. The existence of such a dependence was later questioned by Krishnamurthi et al. (1998) on the basis of their newly determined rotation periods for a sample of Pleiades cluster stars.

Using a sample of stars much larger than that considered by O'Dell et al. and Krishnamurthi et al., we investigate the existence of correlations between $(\Delta V_{\rm as})_{\max}$ (hereafter referred to as $A_{\max}$), the parameter we have chosen as indicator of photospheric magnetic activity confined into spots, and global stellar parameters, such as $B-V$ colour index, rotation rate and other activity indicators.

3.1. Activity-rotation relation

Apart from the field stars, whose interstellar reddening can be neglected because of their proximity to the Sun, all the stars in our sample were first dereddened using the mean $B-V$ colour excess values as used by Pinsonneault et al. (1998). Then, in order to minimise the colour effects (i.e., mass for main sequence stars and convective zone depth) on the activity-rotation relation, we divided our sample into four colour ranges:

$+0.50 \leq B-V \leq +0.57$ (F5−F9)
$+0.58 \leq B-V \leq +0.73$ (G0−G7)
$+0.74 \leq B-V \leq +1.13$ (G8−K4)
$+1.14 \leq B-V \leq +1.70$ (K5−M4).

Each star was assigned to one of the four spectral ranges only on the basis of the $B-V$ colour index.

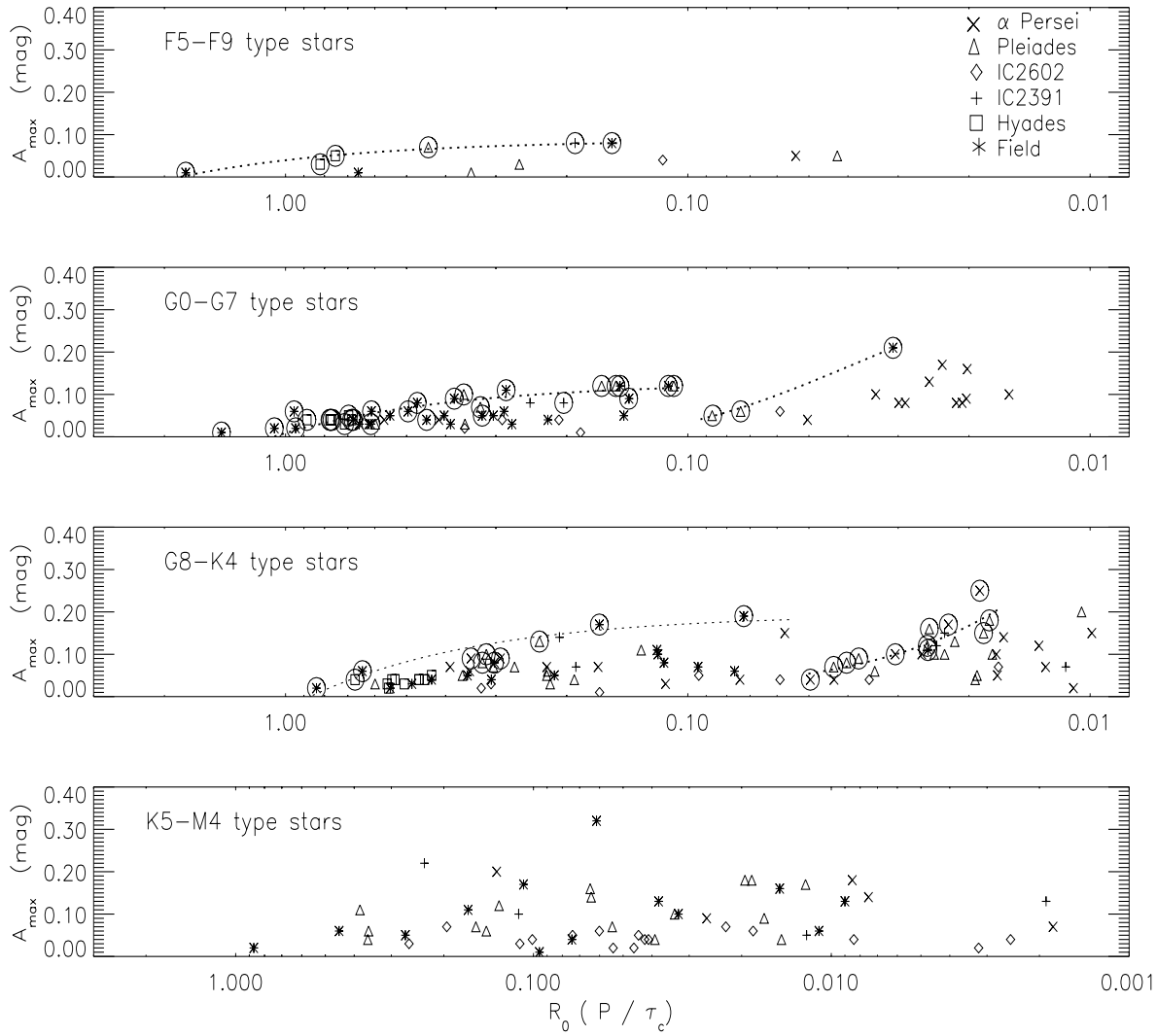

Fig. 4. $A_{\max}$ versus Rossby number (R_0). The data upper envelopes (circled symbols) are fitted (*dotted line*) in the *fast* rotation range by a linear law for F, G and K-type stars. The $A_{\max}$-R_0 relation in the ultra *ultra fast* rotation range is best fitted by a power law for G and K-type stars. Note that the abscissa is logarithmic

Figure 3 shows that the upper envelope of $A_{\max}$ is a decreasing function of the rotation period (P), as expected from the dynamo theory that predicts the magnetic flux density to increase with rotation velocities. However, different quantitative behaviours of the upper envelope of $A_{\max}$ versus P are apparent in the following different rotation rate ranges:

$P \leq 1.10$ (d) (hereafter called *ultra fast* rotators)

$P > 1.10$ (d) (hereafter called *fast* rotators).

The different behaviour in these rotation ranges is best seen among K-type stars (see also Fig. 5), which are the most numerous stars in our sample. We can argue that a similar behaviour may be present in the other mass regimes, but the currently available data are too sparse to support this behaviour as strongly as in the G8-K4 regime. The scatter of $A_{\max}$ at any given rotation period can be due to:

a) the dependence of the magnetic activity on colour, as discussed later on;
b) the different inclination of the rotation axis with respect to the line of sight, as explained in Sect. 2;
c) the paucity of the available light curves for most of the stars in our sample;
d) the different degree of long-term symmetry/asymmetry in the spot distribution.

It can be noted in the ultra fast regime that the $A_{\max}$ upper envelopes of the G and K-type stars (the most numerous in our sample) have their maximum values at about $P \simeq 0.35$ (d) and they do not exceed such values even among the faster rotators ($P \lesssim 0.35$ d). A similar behaviour is more clearly apparent when the Rossby

Table 2. Correlation coefficients (r), number of stars used to define the upper envelope (N), parameters of the linear, exponential and power law weighted fits to the upper data envelope of the $A_{\max}$-P and $A_{\max}$-R_0 relations and reduced chi-squares (χ^2_ν)

Sp. Type	r	N	a	b	χ^2_ν	$\mathrm{Log}_{10}a$	b	χ^2_ν	$\mathrm{Log}_{10}a$	b	χ^2_r
			$A_{\max}=a+bP$			$\mathrm{Log}_{10}A_{\max}=\mathrm{Log}_{10}a+bP$			$\mathrm{Log}_{10}A_{\max}=\mathrm{Log}_{10}a+b\mathrm{Log}_{10}P$		
ultra fast rotation											
G0-G7	−0.99	3	0.23 ± 0.46	-0.33 ± 0.88	2.56	-0.58 ± 0.46	-1.29 ± 0.88	2.76	-0.52 ± 0.45	-1.88 ± 1.31	2.88
G8-K4	−0.89	12	0.25 ± 0.50	-0.23 ± 0.88	0.29	-0.45 ± 0.50	-0.83 ± 0.88	0.21	-1.23 ± 0.35	-1.20 ± 1.25	0.17
fast rotation											
F5-F9	−0.94	6	0.08 ± 0.49	-0.007 ± 0.09	0.15	-1.05 ± 0.50	-0.08 ± 0.09	0.20	-0.98 ± 0.54	-0.75 ± 0.99	0.24
G0-G7	−0.91	29	0.13 ± 0.06	-0.010 ± 0.01	0.30	-0.88 ± 0.06	-0.05 ± 0.01	0.31	-0.75 ± 0.07	-0.58 ± 0.10	0.40
G8-K4	−0.86	10	0.20 ± 0.04	-0.013 ± 0.01	0.50	-0.68 ± 0.05	-0.05 ± 0.01	0.50	-0.60 ± 0.05	-0.60 ± 0.07	0.60
			$A_{\max}=a+bR_0$			$\mathrm{Log}_{10}A_{\max}=\mathrm{Log}_{10}a+bR_0$			$\mathrm{Log}_{10}A_{\max}=\mathrm{Log}_{10}a+b\mathrm{Log}_{10}R_0$		
ultra fast rotation											
G0-G7	−0.90	3	0.21 ± 0.37	-2.04 ± 8.41	2.05	-0.58 ± 0.37	-7.91 ± 8.41	1.13	-0.46 ± 1.55	-1.14 ± 1.08	1.81
G8-K4	−0.86	12	0.25 ± 0.49	-4.76 ± 17.97	0.46	-0.45 ± 0.48	-17.04 ± 15.97	0..30	-2.86 ± 1.86	-1.23 ± 1.16	0.26
fast rotation											
F5-F9	−0.92	6	0.08 ± 0.49	-0.05 ± 0.67	0.16	-1.06 ± 0.49	-0.58 ± 0.67	0.20	-1.03 ± 0.52	-0.75 ± 0.95	0.23
G0-G7	−0.86	29	0.11 ± 0.06	-0.09 ± 0.12	0.25	-0.91 ± 0.06	-0.53 ± 0.12	0.25	-0.74 ± 0.05	-0.60 ± 0.12	0.33
G8-K4	−0.89	10	0.19 ± 0.04	-0.22 ± 0.11	0.43	-0.69 ± 0.04	-0.86 ± 0.11	0.37	-1.33 ± 0.05	-0.53 ± 0.06	0.31

number is used (Fig. 4). The activity-rotation relations are derived by considering the data upper envelopes, which most closely approach the true maximum light curve amplitude at any given rotation period. The stars we used to compute the $A_{\max}$ upper envelope fits are marked by the spectral type ("*fit*") in the last column of Tables 3 to 8 and are represented by circled symbols in the Figs. 3 to 5. The upper envelope of $A_{\max}$ appears to be strongly correlated with both the rotation period and the Rossby number (Table 1 and Fig. 4), with different decreasing slopes in passing from *ultra fast* to *fast* rotators.

The Rossby number R_0 was computed adopting the empirical turnover time given by Noyes et al. (1984) for the $+0.50 \leq B-V \leq +1.36$ colour range (F-K type) and the theoretical turnover time from the Girardi et al. (2000) models for the $+1.37 \leq B-V \leq +1.70$ colour range (M-type).

We argue that the boundary between *ultra fast* and *fast* stars, which is clearest in the G8-K4 regime, falls at the same rotation period for other masses (Fig. 3). Therefore, when $A_{\max}$ is plotted versus Rossby number (R_0) the breaking boundaries would be masked (Fig. 4) by the spurious colour dependence introduced in the normalisation of the rotation period (P) by means of a colour dependent function (τ_c). For this reason the different spectral type ranges are plotted separately in Fig. 4.

Though all the data are lower limits, the discontinuity shown by the upper envelope of $A_{\max}$ in passing from *ultra fast* to *fast* stars (Fig. 5) is unlikely to be an artifact. It is clearly apparent in the K colour range and, even if much less clearly, in the G range. For K-type stars, the discontinuity amplitude (0.20 mag) is almost 20 times larger than

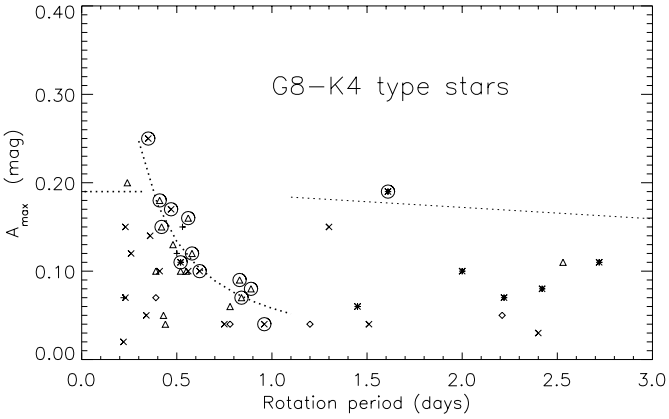

Fig. 5. $A_{\max}$ versus rotation period (P) in the rotation range 0–3 days blown up from Fig. 3 for G8-K4 stars. The symbols have same meaning than in Figs. 3, 4

the standard deviation of the residuals with respect to the data fit for *ultra fast* stars (dotted line in Figs. 4 and 5). For the F stars too few ultra fast rotators are present in our sample to confidently support a similar behaviour.

Because of the detection of this discontinuity in the $A_{\max}$-P relation, a monitoring program of *ultra fast* stars was started. Additional photometry of 21 stars in the Pleiades and Alpha Persei clusters (Messina 2000) confirms that the upper envelope of the maximum V-band light curve amplitudes increases with rotation velocity, within the rotation range 0.4–1.1 days.

The data upper envelopes were fitted by linear, exponential and power law relations. The $A_{\max}$-P relation (both in the *ultra fast* and *fast* rotation ranges) is best

Table 3. Pleiades cluster active stars. The stars that were considered for the $A_{\rm max}$-P upper envelope fits are identified in the last column

Star	Other name	$(B-V)_0$	$P_{\rm rot}$ (d)	$A_{\rm max}$ (mag)	$v\sin i$ (km s^{-1})	R_0	Ref.	# of curves	Notes
HCG20		1.34	2.70	0.15	—	0.130	9	1	
HCG71		1.34	2.98	0.04	—	0.144	9	1	
HII34	V810 Tau	0.88	6.553	0.07	7.3$^{(a)}$	0.304	7	1	
HII133	V623 Tau	1.27	1.36	0.16	9.0	0.064	9	1	
HII152	V936 Tau	0.64	4.12	0.07	11.1$^{(a)}$	0.328	4	1	G_fit
HII191		1.27	3.1	0.04	—	0.145	9	1	
HII250		0.64	0.843	0.06	6.9$^{(a)}$	0.074	8	1	G_fit
HII253		0.64	1.721	0.12	38.2$^{(a)}$	0.151	8	1	G_fit
HII263		0.84	4.82	0.17	10	0.234	9	1	K_fit
HII293		0.66	4.5:	0.03	6.6$^{(a)}$	0.358	6	1	
HII296	V966 Tau	0.82	2.53	0.11	14.7$^{(a)}$	0.131	4	1	
HII314	V1038 Tau	0.62	1.49	0.12	38.0$^{(a)}$	0.164	8	2	G_fit
HII320		0.84	4.6:	0.06	110.8	0.223	6	1	
HII324	V632 Tau	1.00	0.41	0.18	73.0	0.018	5	1	K_fit
HII335	MX Tau	1.22	0.36	0.09	73.0	0.017	5	1	
HII345		0.80	0.84	0.065	18.9$^{(a)}$	0.043	8	2	K_fit
HII357	NP Tau	1.17	3.4:	0.07	7.5	0.156	6	1	
HII625	V811 Tau	1.15	0.428	0.18	94.0	0.019	5	1	
HII686	OU Tau	1.23	0.396	0.18	64.0	0.018	7	2	
HII708	V1085 Tau	0.58	0.294	0.05	46.0	0.042	8	2	
HII727	V855 Tau	0.51	1.2	0.04	50.0	0.262	3	1	
HII738	V1041 Tau	1.13	0.83	0.09	50.0	0.038	9	2	K_fit
HII739	V969 Tau	0.62	0.90	0.05	14.0$^{(a)}$	0.087	8	2	G_fit
HII879	V813 Tau	1.03	7.387	0.08	7.2$^{(a)}$	0.324	7	1	K_fit
HII882		1.03	0.58	0.12	65.0	0.025	7	1	K_fit
HII883	V789 Tau	1.04	7.2	0.10	6:	0.317	9	1	K_fit
HII885		0.97	0.435	0.05	6.1$^{(a)}$	0.019	8	1	
HII930		1.18	1.39	0.14	20	0.064	9	1	
HII975		0.77	4.082	0.05	32.0	0.224	8	1	
HII1032		0.70	1.299	0.12	37.2$^{(a)}$	0.108	8	3	G_fit
HII1039		1.18	0.85:	0.03	5.0$^{(a)}$	0.039	7	1	
HII1124		0.94	6.051	0.07	5.6$^{(a)}$	0.269	7	1	
HII1136	V1065 Tau	0.96	0.52	0.10	60.0	0.023	2	1	
HII1280		1.36	0.302	0.05	—	0.015	9	1	
HII1305		1.11	0.389	0.10	84	0.017	9	1	
HII1332	V815 Tau	0.98	8.30	0.05	2.0$^{(a)}$	0.363	7	1	
HII1512		1.22	8.2	0.12	9	0.382	9	1	
HII1514		0.60	3.28	0.10	13.6$^{(a)}$	0.360	8	1	G_fit
HII1531	QX Tau	1.11	0.483	0.13	50.0	0.022	7	1	
HII1532		1.04	0.78	0.06	6:	0.034	9	1	
HII1653	V338 Tau	1.14	0.74	0.10	21	0.034	9	1	
HII1797		0.52	1.73:	0.01	19.6$^{(a)}$	0.346	7	1	
HII1883	V660 Tau	0.99	0.235	0.20	140.0	0.010	7	3	
HII2034		0.95	0.551	0.10	75.0	0.024	7	1	
HII2244	V664 Tau	0.95	0.565	0.17	50.0	0.025	5	3	K_fit
HII2284	V1089 Tau	0.74	10.1	0.03	3.5$^{(a)}$	0.599	6	1	
HII2341	V1090 Tau	0.68	8.2	0.03	3.4$^{(a)}$	0.598	6	1	
HII2548		1.29	7.5	0.06	10.0	0.358	6	1	
HII2741		0.97	5.00:	0.025	60.0	0.220	3	1	
HII2786		0.52	2.21	0.07	25	0.441	9	1	F_fit
HII2881		0.92	4.25	0.04	7.8$^{(a)}$	0.191	3	1	
HII2927	V378 Tau	1.22	0.262	0.17	95.0	0.012	5	2	
HII2966		1.42	4.6	0.07	$\leq$9	0.054	9	1	
HII3030	V382 Tau	1.35	7.4:	0.04	10.0	0.360	6	1	
HII3063	V677 Tau	1.13	0.89	0.10	26.0	0.040	6	1	K_fit
HII3163	V816 Tau	0.97	0.418	0.15	60.0	0.018	1	2	K_fit
HII3197	V679 Tau	1.03	0.44	0.04	33	0.019	9	1	

(1) Stout-Batalha & Vogt (1999)
(2) Prosser et al. (1993a)
(3) Prosser et al. (1993b)
(4) Magnitskii (1987)
(5) Stauffer et al. (1987)
(:) uncertain
(6) Prosser et al. (1995)
(7) van Leeuwen et al. (1987)
(8) Marilli et al. (1997)
(9) Krishnamurthi et al. (1998)
(a) Queloz et al. (1998).

fitted by a linear law. The $A_{\rm max}$-R_0 relation in the *fast* rotation range is best fitted by a linear law. The $A_{\rm max}$-R_0 relation in the *ultra fast* rotation range is best fitted by a power law for G- and K-type stars (Table 2). All the points in the fits were weighted by the number of light curves used to derive them (see Tables 3–8). The correlation coefficients (r), fit parameters (a and b) and reduced chi-squares (χ^2_ν) are given in Table 2.

Since our analysis is mainly focused on main sequence stars, the IC 2602 and IC 2391 members of spectral type

Table 4. Alpha Persei cluster active stars. The stars that were considered for the $A_{\max}$-P upper envelope fits are identified in the last column

Star	Other name	$(B-V)_0$	$P_{\rm rot}$ (d)	$A_{\max}$ (mag)	$v\sin i$ (km s^{-1})	R_0	Ref.	# of curves	Notes
AP15		1.19	0.64	0.09	52.0	0.026	4	1	
AP37		0.86	2.40	0.03	29.0	0.114	2	2	
AP41		0.61	5.5	0.04	9.0	0.569	9	1	
AP43		0.87	0.56	0.10	72.0	0.026	4	1	
AP56		0.90	0.36	0.14	110.0	0.016	4	1	
AP60		1.60	0.32	0.07	105.0	0.018	3	1	
AP63		0.82	0.22	0.02	161.0	0.011	2	1	
AP70		0.90	6.4	0.09	10.0	0.292	9	2	K_fit
AP72		0.77	6.3	0.09	7.0	0.346	9	1	K_fit
AP86		1.22	0.21	0.18	140.0	0.085	7	3	
AP91		0.83	1.51	0.035	25.0	0.074	3	1	
AP93		0.83	0.62	0.095	79.0	0.030	3	2	K_fit
AP95		0.78	0.35	0.25	140.0	0.019	5	2	K_fit
AP98		0.77	6.2	0.06	7.0	0.349	9	1	
AP100		1.03	0.23	0.15	205.0	0.010	1	3	
AP101		1.14	3.2	0.2	11.0	0.133	9	1	
AP104	HD 19655	0.68	0.41	0.08	10.0	0.030	8	1	
AP114		0.96	1.30	0.15	31.0	0.057	9	1	
AP117		0.85	0.47	0.17	83.0	0.022	2	3	K_fit
AP118	HD 19636	0.71	0.31	0.16	160.0	0.020	1	3	
AP124		1.15	0.18	0.14	190.0	0.007	11	2	
AP127	HD 232762	0.82	0.34	0.05	80.0	0.017	2	1	
AP139		0.80	0.26	0.12	170.0	0.013	1	3	
AP149	HD 19721	0.71	0.32	0.08	117.0	0.021	2	2	
AP156		0.63	4.5	0.04	10.0	0.416	9	1	
AP167	HD 19805	1.13	0.41	0.10	96.0	0.017	10	1	
AP169		0.97	5.1	0.07	8.0	0.416	9	1	
AP193		0.75	0.75	0.04	64.0	0.043	6	1	
AP201		0.94	3.75	0.07	11.0	0.167	9	1	
AP212	HD 19893	0.77	7.1	0.07	6.0	0.390	9	1	
AP225	HD 19908	0.68	0.32	0.17	138.0	0.023	8	3	
AP226	HD 19864	0.76	0.23	0.07	181.02	0.013	2	2	
AP244		0.80	0.96	0.04	42.0	0.050	2	1	K_fit
AP258		0.73	0.26	0.10	170.0	0.016	3	2	
HE373		0.67	0.33	0.13	140.0	0.025	2	2	
HE520	V484 Per	0.69	0.29	0.09	87.0	0.020	4	1	
HE622	V531 Per	0.72	0.80	0.045	61.0	0.051	2	2	
HE684		0.47	0.75	0.065	71.0	0.243	8	2	
HE696		0.66	0.27	0.08	10.0	0.021	8	1	
HE699	V532 Per	0.61	0.33	0.10	90.0	0.034	1	2	
HE709		0.58	0.23	0.08	59.0	0.029	8	1	
HE935		0.52	0.27	0.05	78.0	0.054	8	1	

(1) O'Dell et al. (1993)
(2) Prosser et al. (1993b)
(3) Prosser et al. (1993a)
(4) Stauffer et al. (1985)
(5) Stauffer et al. (1989)
(6) O'Dell et al. (1997)
(7) Stauffer et al. (1987)
(8) Marilli et al. (1997)
(9) Allain et al. (1996)
(10) Prosser et al. (1995)
(11) Bouvier (1996).

later than G8 were excluded from the fitting, because they are pre-main-sequence stars. In the K5-M4 spectral range most of the stars in our sample (all the Alpha Persei and Pleiades as well as a few field stars) have not arrived yet onto the zero-age main-sequence, according to the pre-main-sequence evolutionary tracks computed by D'Antona & Mazzitelli (1994). That means that our K5-M4 sample is not as homogeneous as those discussed before since we have in it stars with quite different convective envelope properties. Therefore, the $A_{\max}$ upper envelope behaviour in this spectral range is not directly comparable with that in the other spectral ranges.

At the first glance, the $A_{\max}$ upper envelope seems to increase at increasing rotation rate up to the highest value of $A_{\max} = 0.32$ mag at $P \simeq 5$ days ($R_0 = 0.06$). Then, it increases less steeply up to a "saturation" level of $A_{\max} = 0.20$ mag. However, such break at 5 days, which is only apparent in the K5-M4 spectral range, cannot be considered real since several stars jump from a rotation regime to the other when the Rossby number is used, which is not the case for the 1.1 days boundary.

The smooth onset of the V-band variability starting from $R_0 < 1$ and the increase of the upper envelope of the light curves maximum amplitude versus smaller Rossby numbers we found in this study is in apparent contradiction with the results of Hall (1991, 1994) and Henry et al. (1995), who found the onset of significant variability at $R_0 < 0.65$ with no obvious increase (decrease) in amplitude down to $R_0 = 0.01$. The apparent contradiction may derive from the use they made of a stellar sample with an extremely large range of global stellar properties. As described in Sect. 3, our analysis instead is focused on a much more homogeneous stellar sample.

Table 5. Hyades cluster active stars. The stars that were considered for the $A_{\rm max}$-P upper envelope fits are identified in the last column

Star	Other name	$(B-V)_0$	$P_{\rm rot}$ (d)	$A_{\rm max}$ (mag)	$v\sin i$ (km s^{-1})	R_0	Ref.	# of curves	Notes
VB21	V984 Tau	0.816	8.98	0.038	—	0.450	2	1	
VB25	V985 Tau	0.987	12.64	0.023	—	0.554	1	1	
VB26	V893 Tau	0.743	9.39:	0.038	—	0.552	1	1	
VB31	V986 Tau	0.566	5.44	0.049	10.0	0.752	1	1	F_fit
VB43	V998 Tau	0.907	10.26	0.045	—	0.466	1	1	
VB50	V895 Tau	0.601	7.10	0.035	—	0.775	2	1	G_fit
VB52	V897 Tau	0.597	7.90	0.042	6.0	0.881	2	1	G_fit
VB59	V992 Tau	0.543	4.98	0.032	6.0	0.820	1	1	F_fit
VB63	V906 Tau	0.632	7.8	0.034	7.1	0.713	2	1	G_fit
VB64	V911 Tau	0.657	8.67	0.035	5.1	0.699	1	1	G_fit
VB69	V918 Tau	0.746	11.52	0.044	—	0.672	2	1	K_fit
VB73	V920 Tau	0.609	7.63	0.039	7.0	0.794	1	1	G_fit
VB79		0.831	11.38	0.032	—	0.559	1	1	
VB91	V996 Tau	0.883	9.36	0.051	—	0.433	1	1	
VB92	V997 Tau	0.741	9.04	0.041	—	0.534	1	1	
VB97	V938 Tau	0.634	8.55	0.035	—	0.773	2	1	G_fit
VB102	V998 Tau	0.603	6.46	0.046	7.0	0.697	1	1	G_fit
VB173	V989 Tau	1.237	14.14	0.034	—	0.569	1	1	
VB175	V991 Tau	1.031	10.82	0.036	—	0.465	1	1	
VB174	V990 Tau	1.058	11.88	0.032	—	0.507	1	1	
VB181	V995 Tau	1.167	11.92	0.040	—	0.491	1	1	

(1) Radick et al. (1987) (2) Lockwood et al. (1984)
(:) uncertain period.

Table 6. IC 2391 cluster active stars (Patten & Simon 1996). The stars that were considered for the $A_{\rm max}$-P upper envelope fits are identified in the last column

VXR	Other name	$(B-V)_0$	$P_{\rm rot}$ (d)	$A_{\rm max}$ (mag)	$v\sin i$ (km s^{-1})	R_0	# of curves	Notes
12	SHJM 6	0.83	3.86	0.07	16	0.189	2	
14		0.56	1.32	0.08	—	0.191	2	F_fit
35a		0.99	0.527	0.15	90	0.023	1	
38a	SHJM 3	1.23	2.78	0.10	18	0.111	2	
41	SHJM 8	1.25	5.80	0.22	$\leq$15	0.231	2	
42a	SHJM 9	1.54	1.81	0.05	—	0.066	1	
45a		0.80	0.223	0.07	—	0.011	1	
47		1.43	0.258	0.13	95	0.002	1	
60a	SHJM 10	—	0.93:	0.09	$\leq$15	—	1	
60b	SHJM 4	—	0.212	0.10	150	—	1	
62a	SHJM 5	0.85	0.503:	0.12	—	0.024	1	
64a		—	0.543	0.05	—	—	1	
70		0.63	2.67	0.08	—	0.246	1	G_fit
72		0.72	3.23	0.08	—	0.203	1	
76a		1.04	4.86	0.14	—	0.208	1	
77a		0.50	0.653	0.07	—	0.177	1	

(:) uncertain period.

The existence of a discontinuity in passing from *ultra fast* to *fast* rotating stars may be attributed to an abrupt change of the total spotted areas or of their spatial redistribution and would imply different efficiency or different operation mode of the dynamo action when operating at rather different rotation regimes.

3.2. Saturation

Chromospheric, TR and coronal emission fluxes show evidence of saturation, i.e., a progressive flattening of their activity rate increase with advancing rotation rate, at $R_0 \simeq 0.33$ for chromospheric fluxes and at slightly larger values, $R_0 \simeq 0.5{-}0.7$, for TR and coronal fluxes (Vilhu 1984).

Several causes may be responsible for the observed saturation, such as:

a) the filling of the entire atmosphere by magnetic regions ($f \rightarrow 1$);

b) a negative feedback on the convective motions and on the differential rotation due to the widespread presence of intense magnetic fields (Robinson & Durney 1982);

c) a saturation of the emission mechanism efficiency.

We find evidence that the upper envelope of the $A_{\rm max}$-P correlation stops increasing at rotation periods $P \lesssim 0.35$ days (Fig. 5) and, similar to the results of

Table 7. IC 2602 cluster active stars (Barnes et al. 1999). The stars that were considered for the $A_{\rm max}$-P upper envelope fits are identified in the last column

Name	$(B-V)_0$	$P_{\rm rot}$ (d)	$A_{\rm max}$ (mag)	$v\sin i$ (km s^{-1})	R_0	# of curves	Notes
B134	0.91	6.8	0.025	10	0.308	1	
W79	0.79	6.2	0.02	8	0.326	1	
R15	0.89	3.6:	0.01	7	0.166	1	
R24A	1.39	1.25	0.06	34	0.018	1	
R26	1.50	5.7	0.05	6	0.044	1	
R27	1.46	4.5:	0.035	10	0.166	1	
R29	1.07	2.21	0.05	22	0.042	1	
R31	1.55	0.49	0.02	35	0.003	1	
R32	1.59	4.0	0.075	9	0.023	1	
R43	0.90	0.78	0.035	50	0.035	1	
R44	1.50	5.5	0.04	7	0.041	1	
R50	1.51	6.4	0.02	7	0.046	1	
R52	1.02	0.393	0.07	95	0.017	1	
R53B	1.57	0.41	0.045	100	0.002	1	
R56	1.39	4.1	0.055	17	0.060	1	
R57	1.56	8.7	0.02	6	0.054	1	
R58	0.60	0.57	0.055	93	0.059	1	
R66	0.64	3.3	0.035	12	0.289	1	
R70	0.65	4.3	0.02	11	0.359	1	
R72	0.59	1.05	0.035	49	0.115	1	
R77	1.43	10.1	0.03	7	0.111	1	
R83	0.58	1.67	0.035	30	0.209	1	
R88A	1.16	0.204	0.04	200	0.008	1	
R89	1.20	4.8	0.065	14	0.195	1	
R92	0.63	2.0:	0.015	14	0.185	1	
R93	1.33	6.7	0.025	8	0.262	1	
R94	1.35	2.6	0.035	23	0.101	1	
R95A	0.83	1.20	0.04	12	0.059	1	
R96	1.21	1.82	0.05	17	0.074	1	

(:) uncertain period.

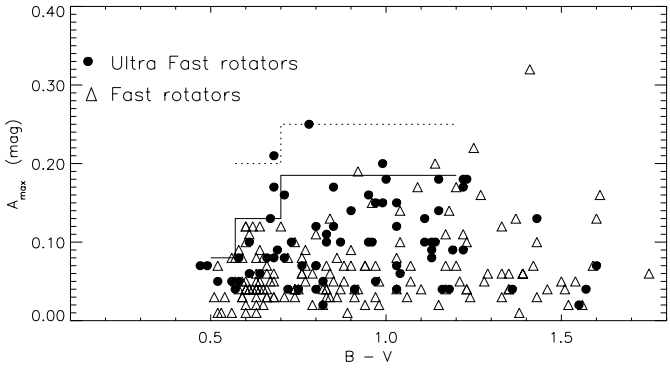

Fig. 6. The light curve maximum amplitude versus $B-V$ colour. Continuous and dotted horizontal lines indicate the offset values (parameter a in Table 2) of the linear fits to the $A_{\rm max}$-P relation for *fast* and *ultra fast* stars, respectively

O'Dell et al. (1995), at Rossby numbers $R_0 \lesssim 0.018$. The lack of correlation between $A_{\rm max}$ and P, at very high rotation rates may be simply due to an underestimated $A_{\rm max}$ upper envelope, since it is a lower limit. However, as is clear when R_0 is used (Fig. 4; see also O'Dell et al. 1995), we may tentatively infer the presence of "saturation". By this, we mean that either the dynamo stops producing more spots, or it produces additional spots in such a way that $A_{\rm max}$ does not increase (e.g., by evenly distributing them).

If our hypothesis of a saturation effect is correct, since such saturation appears at values of R_0 ($R_0 < 0.02$) orders of magnitude smaller than the values at which chromospheric, TR's and coronal emission fluxes saturate ($R_0 < 0.33$), the spot covering fraction appears to be a more suitable indicator of the magnetic dynamo activity at R_0 values ($0.02 < R_0 < 0.33$), i.e. below the values where activity flux saturation occurs. The lack of detection of a saturation regime by Krisnamurthi et al. (1998) may possibly be due to the less numerous fast rotators they had in their stellar sample.

3.3. Color and age dependence

As shown in Figs. 3 and 6, the photospheric activity level measured by the maximum light curve amplitude depends on the star's color. Both ultra fast and fast rotating K-type stars reach an activity level (as shown by the data upper envelope) higher than F-, and G-type stars of same rotation period. The dependence on the $B-V$ colour (Fig. 6) is very similar in both rotation ranges. Continuous and dotted horizontal lines indicate the offset values (parameter a in Table 2) of the linear fits to the $A_{\rm max}$-P relation for *fast* and *ultra fast* stars, respectively.

The cluster ages we are considering in our sample are in the range 0.03 Gyr (IC 2602 and IC 2391 clusters) to 0.6 Gyr (Hyades cluster). As shown in Fig. 3, in the F, G and K spectral range the value of the upper envelope is determined mainly by the Pleiades cluster and field stars, most of which belong to the Pleiades cluster moving group. Therefore, it seems that the spot activity level on the main sequence increases from the zero-age main sequence, with its maximum level around the Pleiades age (0.07 Gyr), and

Table 8. Field active stars. The stars that were considered for the $A_{\max}$-P upper envelope fits are identified in the last column

Star	Other name	$B-V$	$P_{\rm rot}$ (d)	$A_{\max}$ (mag)	$v\sin i$ (km s^{-1})	R_0	Ref.	# of curves	Notes
HD 987		0.71	4.2	0.03	10	0.273	17	1	
HD 1835[a]	BE Cet	0.66	7.655	0.05	–	0.609	20,2	25	*G_fit*
HD 7172		0.63	3.1	0.06	13	0.286	17	1	
HD 17925	EP Eri	0.87	6.57	0.04	≤ 8	0.308	2	3	
HD 18134	VZ Hor	0.74	2.0	0.10	–	0.135	11	1	
HD 18632	BZ Cet	0.66	10.22	0.02	1.8	0.813	13	1	*G_fit*
HD 20630	κ^1 Cet	0.68	9.0	0.03	3.8	0.656	2	3	
HD 21845	V577 Per	0.79	1.454	0.06	–	0.076	2	3	
HD 25893	V491 Per	0.85	7.37	0.05	4.5	0.353	12	3	
HD 26913	V891 Tau	0.68	6.8	0.06	3.9	0.496	8	4	*G_fit*
HD 29697	V834 Tau	1.09	3.936	0.17	9.5	0.167	13	2	*K_fit*
HD 31993	V1192 Ori	1.28	6.78	0.05	31.1	0.269	14	1	
HD 35296	V111 Tau	0.53	3.6	0.01	15.4	0.660	29,10	2	
HD 36705	AB Dor	0.83	0.5146	0.11	85	0.025	14,1	6	*K_fit*
HD 36869		0.64	1.31	0.09	28	0.140	22,1	2	*G_fit*
HD 37394		0.84	10.00	0.03	4.0	0.485	2	1	
HD 37572	UY Pic	0.82	4.3:	0.05	9	0.214	1	1	
HD 39587[a]	χ^1 Ori	0.59	5.24	0.03	9	0.621	2	21	*G_fit*
HD 42807		0.66	7.8	0.03	–	0.621	10	1	
HD 43989	V1358 Ori	0.57	1.15	0.08	47	0.154	22	2	*F_fit*
HD 45081	AO Men	1.20	2.65	0.17	17	0.108	1	2	
HD 52452		0.68	0.423	0.21	15	0.031	2	6	*G_fit*
HD 64096	9 Pup	0.60	9.7	0.02	8	1.066	10	1	*G_fit*
HD 70573		0.63	3.296	0.05	13.6	0.304	13	1	
HD 72905[a]	π^1 Uma	0.60	4.5395	0.04	9.5	0.502	2	10	*G_fit*
HD 78644		0.64	4.6:	0.05	59	0.402	1	1	
HD 82443[a]	DX Leo	0.76	5.377	0.08	6.5	0.304	9	15	*K_fit*
HD 82558[a]	LQ Hya	0.92	1.61	0.19	26	0.073	15	23	*K_fit*
HD 88230		1.38	6.0:	0.01	3.1	0.095	3	1	
HD 95650	DS Leo	1.43	2.94	0.10	–	0.033	16	1	
HD 98712	SZ Crt	1.36	11.58	0.06	–	0.448	23,1	5	
HD 114710	β Com	0.56	12.26	0.01	4.3	1.771	4	1	*F_fit*
HD 115383[a]	59 Vir	0.59	3.328	0.03	3	0.386	2	19	*G_fit*
HD 115404		0.94	18.8	0.02	3.9	0.838	3	1	
HD 118100	EQ Vir	1.17	4.03	0.11	13	0.164	21,19	4	
HD 129333[a]	EK Dra	0.61	2.787	0.10	–	0.283	2	26	*G_fit*
HD 134319[a]	IU Dra	0.68	4.448	0.04	–	0.324	6	10	*G_fit*
HD 140637	KW Lup	1.02	2.72	0.11	14	0.119	22	1	
HD 149661	12 Oph	0.82	11.0	0.02	0.6	0.549	18	1	
HD 152391[a]	V2292 Oph	0.76	11.45	0.06	3.7	0.644	2	21	*K_fit*
HD 156026	V2215 Oph	1.15	21.0:	0.02	2.2	0.869	14	1	
HD 160934		1.23	1.842	0.02	16.4	0.074	13	1	
HD 171488	V889 Her	0.60	1.341	0.12	40	0.123	2	6	*G_fit*
HD 190406	15 Sge	0.60	13.95	0.01	4	1.443	2	3	*G_fit*
HD 197481	AU Mic	1.44	4.9	0.32	–	0.061	24,7	10	
HD 206860	HN Peg	0.59	4.70	0.05	11	0.550	2	2	
HD 216803	TW Psa	1.10	10.3	0.04	–	0.433	5	1	
HD 234601[a]		0.63	7.35	0.04	7	0.679	30	9	*G_fit*
HD 295290		0.58	3.04:	0.09	–	0.380	1	1	*G_fit*
SAO 45568		0.59	8.13	0.06	–	0.942	2	10	*G_fit*
SAO 51891	V383 Lac	0.86	2.42	0.08	19.8	0.114	13	1	
SAO 150508		0.67	1.895	0.05	20	0.144	1	1	
	GT Peg	1.6	1.64	0.13	–	0.009	25,7	1	
	V1005 Ori	1.37	1.90	0.13	–	0.038	26,7	1	
	V1285 Aql	1.75	2.9	0.06	–	0.011	27,7	1	
	YZ CMi	1.61	2.8	0.16	–	0.015	28,7	1	
EXO 052707	−3329.2	1.07	2.22	0.07	40	0.094	17	2	
1E2349.8-0112	BS Psc	0.62	1.145	0.12	47.3	0.111	13	1	
HE 628		0.65	2.676:	0.045	–	0.230	31	1	
HE 1150		0.62	5.64	0.08	–	0.470	31	1	*G_fit*

(1) Cutispoto & Messina, *person. comm.*
(2) Messina 1998, Ph.D. Thesis
(3) Chugainov (1991)
(4) Dorren et al. (1993), *person. comm.*
(5) Vogt (1975)
(6) Messina et al. (1999a)
(7) Alekseev & Gershberg (1996)
(8) Ziegler et al. (1984)
(9) Messina et al. (1999b)
(10) Stepien & Geyer (1996)
(*a*) star in Fig. 2
(11) Eggen (1984)
(12) Strassmeier et al. (1989)
(13) Henry et al. (1995)
(14) Lloyd Evans & Koen (1987)
(15) Oláh et al. (2000)
(16) Bopp et al. (1983)
(17) Cutispoto et al. (1996)
(18) Dorren & Guinan (1982)
(19) Anderson (1979)
(20) Chugainov (1980)
(:) uncertain period
(21) Torres & Ferraz-Mello (1971)
(22) Cutispoto et al. (1999)
(23) Torres et al. (1985)
(24) Torres et al. (1972)
(25) Bopp & Evans (1973)
(26) Bopp et al. (1978)
(27) Byrne et al. (1984)
(28) Chugainov (1974)
(29) Donahue (1993)
(30) Cutispoto et al. (2000) *in press*
(31) Marilli et al. (1997).

then decreases. In the M spectral range, where most of the stars are in the pre-main sequence evolutionary stage, the spot activity level appears to be somehow higher than on the main sequence.

3.4. Activity-flux relation

Activity diagnostics formed at various temperature regimes or atmospheric levels are strongly correlated each other. The flux-flux relations are best fitted by power laws with steepening slopes when increasingly high temperature diagnostics are plotted against the coolest ones (Rutten et al. 1991; Piters et al. 1997; Ayres et al. 1995; Marilli & Catalano 1984). These relations still hold when stars of different spectral type, luminosity class and multiplicity are considered, indicating that the activity structures are temporally and possibly spatially correlated at all atmospheric levels. These correlations are similar for a wide variety of stellar parameters.

The dependence of spot activity upper envelope on the rotation period for "fast" G stars was then compared with the rotational dependence of other activity indicators in the corona, TR and chromosphere: X-ray, Mg II h&k and C IV luminosity, respectively. In our analysis we used the luminosity-rotation relations of Dorren et al. (1994), because all the stars we used to define the upper envelope of G-type *fast* stars (last column of Tables 3–8) have the same global properties (G0-G7 spectral range, rotation period longer than ∼1.1 days, and age of the Pleiades, or older) of those analysed by Dorren et al. within the "Sun in Time" project at the Villanova University (Dorren et al. 1994; Dorren & Guinan 1994; Guinan et al. 1995) and from which the relations between X-ray, Mg II h&k and C IV luminosity and rotation period were derived. Hence, most of the best observed G-type *fast* stars were selected just from the "Sun in Time" stellar sample. The following mean relations are found to apply:

$$L_{\rm X} \propto P^{-2.01} \quad (3)$$

$$L_{\rm CIV} \propto P^{-1.50} \quad (4)$$

$$L_{\rm MgII} \propto P^{-0.94} \quad (5)$$

$$A_{\rm max} \propto P^{-0.58} \quad (G\text{-}type\ fast\ stars). \quad (6)$$

The relations (3), (4) and (5) were derived from the data in Table 3 of Dorren et al. (1994), the relation (6) is from Table 2.

On the basis of the strong correlation between the photospheric and upper layers' activity diagnostics and the rotation period, we expect that a relation should also exist between the $A_{\rm max}$ upper envelope and the upper layers' activity diagnostics. By folding Eqs. (3–6) we may predict the following relations:

$$L_{\rm X} \propto A_{\rm max}^{3.41} \quad (7)$$

$$L_{\rm CIV} \propto A_{\rm max}^{2.54} \quad (8)$$

$$L_{\rm MgII} \propto A_{\rm max}^{1.59} \quad (9)$$

or

$$L_{\rm X} \propto L_{\rm CIV}^{1.34} \propto L_{\rm MgII}^{2.14} \propto A_{\rm max}^{3.41}. \quad (10)$$

However, it must be stressed that such relations are just predicted and must be considered very tentative since they are folded and obtained by substituting the upper envelope relation for our sample of fast G0-G7 type stars into relations for a much larger sample of G0-G8 stars, of which our upper envelope fast stars are only a small fraction.

4. Conclusion

We have presented an extension down to the photosphere of the *rotation-activity connection*, so far extensively studied and well established for the outermost atmospheric layers. It is shown that the envelope of the maximum light curve amplitude in the V-band ($A_{\rm max}$) can be adopted as an indicator of a lower limit of the photospheric magnetic filling factor ($f_{\rm S}$) and, therefore, as a measure of a lower limit of the photospheric magnetic activity confined into spots. The study of the photospheric magnetic activity by means of $A_{\rm max}$ in a sample of 225 field and cluster active stars, which is much larger than previously analysed (O'Dell et al. 1995; Krishnamurthi et al. 1998), reveals the existence of different behaviours of the $A_{\rm max}$-P correlation in different rotation rate ranges. At the base of these behaviours may reside a different dynamo efficiency, which effectively operates within a limited rotation range. Moreover, the absence of correlation in the $A_{\rm max}$-P relation, at very high rotation rates, and Rossby numbers $R_0 \leq 0.02$, may be tentatively interpreted as a saturation effect. We believe that saturation is a regime in which the dynamo can produce the widest range of distribution of $A_{\rm max}$ values from very small to maximum. In the case the hypothesis of the existence of a saturation regime is correct, since the value of R_0 at which $A_{\rm max}$ saturates is orders of magnitude smaller than the value at which chromospheric, TR's and coronal emission fluxes saturate, the spot covering fraction would be the most reliable indicator of magnetic dynamo activity at rotation rates above those where activity fluxes saturate.

The activity level, as measured by the envelope of the maximum light curve amplitudes, appears to depend also on the $B-V$ colour and age. The maximum activity level is found in the K spectral range and at the Pleiades cluster age, for both *fast* and *ultra fast* stars. The remarkable photospheric activity level on K stars, relative to other spectral types, has been suggested more than two decades, when early evidence concerning a small sample of active RS CVn-type binaries was presented (Catalano et al. 1980). Our results are based on a much larger stellar sample. Hence, we can conclude with confidence that the highest dynamo efficiency, at least in producing asymmetric spot distributions, and the best observation conditions for photospheric activity development and manifestations at the main sequence age are met in K-type stars.

At the pre-main sequence evolutionary stage the spot activity level appears somehow higher than for main sequence stars.

On the basis of the strong correlation between the photospheric and upper layers' activity diagnostics and the rotation period, we tentatively predict that a relation should also exist between the $A_{\max}$ upper envelope and the upper layers' activity diagnostics (see Eq. (10)). This aspect certainly deserves to be more deeply investigated and tested by using data in the literature and new data bases.

Acknowledgements. The authors are very grateful to the referee Dr. S. Saar for very careful reading and several helpful suggestions for improving the manuscript. S. Messina is also grateful to Dr. L. Girardi for kindly computing and making available to us the internal structure models for M-type stars.

The extensive use of the SIMBAD and ADS databases operated by the CDS center, Strasbourg, France, is also gratefully acknowledged.

Active star research at the Department of Physics and Astronomy of Catania University and Catania Astrophysical Observatory is funded by MURST (*Ministero dell'Università e della Ricerca Scientifica e Tecnologica*), CNAA (*Consorzio Nazionale per l'Astronomia e l'Astrofisica*) and the *Regione Siciliana*, whose financial support is gratefully acknowledged.

References

Alekseev, I. Y., & Gershberg, R. E. 1996, Astron. Reports, 40, 538
Allain, S., Fernandez, M., Martin, E. L., & Bouvier, J. 1996, A&A, 314, 173
Anderson, C. M. 1979, PASP, 91, 202
Ayres, T. R., Fleming, T. A., Simon, T., et al. 1995, ApJS, 96, 223
Barnes, S. A., Sofia, S., Prosser, C. F., & Stauffer, J. R. 1999, ApJ, 516, 263
Bopp, B. W., & Evans, D. S. 1973, MNRAS, 154, 343
Bopp, B. W., Torres, C. A. O., Busko, I. C., & Quast, G. R. 1978, IBVS, 1443
Bopp, B. W., Africano, J. L., Stence, R. E., Noha, P. V., & Klimke, A. 1983, AJ, 275, 691
Bouvier, J. 1996, A&AS, 120, 127
Byrne, P. B., Doyle, J. G., Butler, C. J., & Andrews, A. D. 1984, MNRAS, 211, 607
Byrne, P. B., Panagi, P. M., Lanzafame, A. C., et al. 1995, A&A, 299, 115
Catalano, S., Frisina, A., & Rodonò, M. 1980, in Symp. IAU 88, Close binary stars: Observations and interpretation, ed. M. J. Plavec, D. M. Popper, & R. K. Ulrich (Dordrecht: Reidel), 405
Chugainov, P. F. 1974, Izv. Krimskoi Astrofiz. Obs., 54, 3
Chugainov, P. F. 1980, Izv. Krimskoi Astrofiz. Obs., 61, 124
Chugainov, P. F. 1991, in Angular Momentum Evolution of Young Stars, ed. S. Catalano, & R. J. Stauffer (Kluwer), 175
Cutispoto, G., Tagliaferri, G., Pallavicini, R., Pasquini, L., & Rodonò, M. 1996, A&AS, 115, 41
Cutispoto, G., Pastori, L., Tagliaferri, G., Messina, S., & Pallavicini, R. 1999, A&AS, 138, 87
Cutispoto, G., Pastori, L., Guerrero, A., et al. 2000, A&A, in press
D'Antona, F., & Mazzitelli, I. 1994, ApJS, 90, 467
Donahue, R. 1993, Ph.D. Thesis, New Mexico State University
Dorren, J. D., & Guinan, E. F. 1982, AJ, 87, 1546
Dorren, J. D., & Guinan, E. F. 1994, ApJ, 428, 805
Dorren, J. D., Guinan, E. F., & DeWarf, L. E. 1994, in ASP Conf. Ser. 64, Cool stars, Stellar Systems and the Sun, ed. J.-P. Caillaut, 399
Eggen, O. J. 1984, AJ, 89, 1358
Girardi, L., Bressan, A., Bertelli, G., & Chiosi, C. 2000, A&AS, 141, 371
Guinan, E. F., DeWarf, L. E., Messina, S., & McCook, G. P. 1995, BAAS, 186, 2101
Hall, D. S. 1991, in Coll. IAU 130, The Sun and Cool Stars. Activity, Magnetism and Dynamos, ed. I. Tuominen, D. Moss, & G. Rudiger (Springer-Verlag), 353
Hall, D. S. 1994, Mem. Soc. Astron. It., 65, 73
Henry, G. W., Fekel, F. C., & Hall, D. S. 1995, AJ, 110, 2926
Kopp, G., & Rabin, D. 1992, Sol. Phys., 141, 253
Krishnamurthi, A., Terndrup, D. M., Pinsonneault, M. H., et al. 1998, ApJ, 493, 914
Lanza, A. F., Catalano, S., Cutispoto, G., Pagano, I., & Rodonò, M. 1998, A&A, 332, 541
Lloyd Evans, T., & Koen, M. C. J. 1987, South Afr. Obs. Circ., 11, 21
Lockwood, G. W., Thompson, D. T., Radick, R. R., et al. 1984, PASP, 96, 714
Magnitskii, A. K. 1987, Sov. Astron. Lett., 13, 451
Marilli, E., & Catalano, S. 1984, A&A, 133, 57
Marilli, E., Catalano, S., & Frasca, A. 1997, Mem. Soc. Astron. Ital., 68, 895
Mathys, G. 1989, Fundamen. Cosm. Phys., 13, 143
Messina, S. 1998, Ph.D. Thesis, Univ. of Catania, Italy
Messina, S., Guinan, E. F., & Lanza, A. F. 1999a, Ap&SS, 260, 493
Messina, S., Guinan, E. F., Lanza, A. F., & Ambruster, C. 1999b, A&A, 347, 249
Messina, S. 2000, submitted to A&A
Neff, J. E., O'Neal, D., & Saar, S. H. 1995, ApJ, 452, 879
Noyes, R. W., Hartmann, L., Baliunas, S. L., Dunkan, D. K., & Vaughan, A. H. 1984, ApJ, 279, 763
O'Dell, M. A., & Collier Cameron, A. 1993, MNRAS, 262, 521
O'Dell, M. A., Panagi, P., Hendry, M. A., & Collier Cameron, A. 1995, A&A, 294, 715
O'Dell, M. A., Hilditch, R. W., Collier Cameron, A., & Bell, S. A. 1997, MNRAS, 284, 874
Oláh, K., Kolláth, Z., & Strassmeier, K. G. 2000, A&A, 356, 643
O'Neal, D., Saar, S. H., & Neff, J. E. 1996, ApJ, 463, 766
O'Neal, D., Saar, S. H., & Neff, J. E. 1998, ApJ, 501, L73
Pallavicini, R. 1992, in The Sun as a Laboratory for Astrophysics, ed. J. T. Schmeltz, & J. C. Brown (Dordrecht: Kluwer), 313
Parker, E. N. 1979, Cosmic Magnetic Fields, their Origin and Activity (Oxford: Clarendon Press)
Patten, B. M., & Simon, T. 1996, ApJS, 106, 489
Pinsonneault, M. H., Stauffer, J., Soderblom, D. R., King, J. R., & Hanson, R. B. 1998, ApJ, 504, 170
Piters, A. J. M., Schrijver, C. J., Schmitt, J. H. M. M., et al. 1997, A&A, 325, 1115
Prosser, C. F., Schild, R. E., Stauffer, J. R., & Jones, F. J. 1993a, PASP, 105, 269

Prosser, C. F., Shetrone, M. D., Marilli, E., et al. 1993b, PASP, 105, 1407
Prosser, C. F., Dasgupta, A., Baknam, D. E., et al. 1995, PASP, 107, 211
Queloz, D., Allain, S., Mermilliod, J.-C., Bouvier, J., & Mayor, M. 1998, A&A, 335, 183
Radick, R. R., Thompson, D. T., Lockwood, G. W., Dunkan, D. K., & Baggett, W. E. 1987, ApJ, 321, 459
Radick, R. R., Lockwood, G. W., & Baliunas, S. L. 1989, Science, 247, 39
Radick, R. R., Lockwood, G. W., Skiff, B. A., & Baliunas, S. L. 1998, ApJS, 118, 239
Robinson, R. D., & Durney, B. R. 1982, A&A, 108, 322
Rodonò, M., Lanza, A. F., & Catalano, S. 1995, A&A, 301, 75
Rutten, R. G. M., Schrijver, C. J., Lemmens, A. F. P., & Zwaan, C. 1991, A&A, 252, 203
Saar, S. H. 1990, in Solar Photosphere: Structure, Convection and Magnetic Fields, ed. J. O. Stenflo (Dordrecht: Kluwer), 427
Saar, S. H. 1996, in Coll. IAU 153, Magnetodynamics Phenomena in the Solar atmosphere - Prototypes of Stellar Magnetic Activity, ed. Y. Uchida, T. Kosugi, & H. S. Hudson (Kluwer), 367
Schüssler, M. 1983, in Symp. IAU 102, Solar and stellar magnetic fields, ed. J. O. Stenflo (Dordrecht: Reidel), 213
Stauffer, J. R., Hartmann, L. W., Birnham, J. N., & Jones, B. F. 1985, ApJ, 289, 247
Stauffer, J. R., Schild, R. E., Baliunas, S. L., & Africano, J. L. 1987, PASP, 99, 471
Stauffer, J. R., Hartmann, L. W., & Jones, B. F. 1989, ApJ, 346, 160
Stepien, K., & Geyer, E. 1996, A&AS, 117, 83
Stout-Batalha, N. M., & Vogt, S. S. 1999, ApJS, 123, 251
Strassmeier, K. G., Hall, D. S., Boyd, L. J., & Genet, R. M. 1989, ApJS, 69, 141
Torres, C. A. O., & Ferraz-Mello, S. 1971, IBVS, 577
Torres, C. A. O., Ferraz-Mello, S., & Quast, G. R. 1972, Astrophys. Lett., 11, 13
Torres, C. A. O, Busko, I. C., & Quast, G. R. 1985, Rev. Mex. Astron. Astrofis., 10, 329
Van Leeuwen, F., Alphenaar, P., & Meys, J. J. M. 1987, A&AS, 67, 483
Vilhu, O. 1984, A&A, 133, 117
Vogt, S. S. 1975, ApJ, 199, 418
Ziegler, K., Shirley, M., Francam, B., Florence, W., & Hall, D. S. 1984, IBVS, 2619